EAST EUROPEAN JOURNAL OF PHYSICS. 3. 391-399 (2023)
DOI:10.26565/2312-4334-2023-3-42 ISSN 2312-4334

INVESTIGATION OF STRUCTURAL, OPTICAL AND ELECTRICAL PROPERTIES OF MnO DOPED WITH Cu THIN FILMS PREPARED BY PLD TECHNIQUE FOR SOLAR CELL APPLICATIONS†

Doaa T. Mohammed*, Ghuson H. Mohammed
Department of Physics, College of Science, University of Baghdad, Baghdad, Iraq
**Corresponding Author e-mail: duaathamer111@gmail.com*
Received June 9, 2023; revised June 24, 2023; accepted June 26, 2023

In the current study, concentrated Nd:YAG laser pulses at 500 mJ with a second radiation at 1064 nm (pulse width 9 ns) and repetition frequency (6 Hz) for 300 laser pulses incident on the target surface were employed to coat glass substrates with MnO thin films. Using an X-ray diffractometer (XRD), an atomic force microscope (AFM), and a UV-Vis spectrophotometer, the structural, morphological, and optical characteristics of the films doped with different concentrations of Cu content (0.03, 0.05, 0.07, and 0.09) were examined. The results show that the films are polycrystalline, with the largest peak appearing at an angle of 35.31, or a reflection of (111). The crystalline size of the deposited thin films was calculated using Debye Scherer formula and found to increase from 11.8 nm for undoped MnO_2 to 29.6 nm for doped (MnO) with the increase of Cu content from x=0 to x=0.09 at preferred orientation of (111). All the samples have a cubic structure. Also, the results showed that Cu content of the films affects the surface morphology. From the results of AFM analysis, it was found that the roughness and average diameter change when adding Cu to the structure, with the highest value occurring at Cu ratio 0.09 equal to 65.40 and 71.21 nm, respectively. UV–Vis spectrophotometer was used to investigate the optical transmission. It was found that when Cu content of films increased, the transmittance of films decreased. Hall Effect measurements show that all prepared films at RT have two type of conductivity P-type and n-type. The electrical characteristics of the $(MnO)_{1-x}Cu_x$/Si heterojunction Solar Cell have been studied and found that the efficiency (η) decreases with the increase of Cu content.
Keywords: *Cu Nanoparticles; MnO Thin Films; PLD Technique; Structural Properties; Optical Properties*
PACS: 73.61.-r, 61.05.C-, 61.05.cc, 61.05.cf, 61.05.cj, 75.70.Ak, 78.20.Ci

1. INTRODUCTION

The use of thin film semiconductors has generated significant interest in a growing range of applications in various electrical and optoelectronic devices due to their low production costs, and thin film technology has a major position in basic research. An examination of the literature reveals that numerous research teams have studied thin-film technology. As a result, a number of deposition processes have emerged, the majority of which depend on continuous, high-temperature power sources [1]. Nanoparticles are the fundamental structures in nanotechnology, which has many applications in different areas such as biosensor and electronic nanodevices [2]. An important class of nanostructured materials are the metal oxide thin films. It is possible to create the thin film's nanomaterials and grown using various methods. There are several widely used methods for depositing thin films onto a substrate, including pulsed laser deposition [3], chemical vapor deposition [4-5] reactive magnetron sputtering [6], spray pyrolysis [7], atomic layer deposition [8], chemical bath deposition [9] and so on. Manganese dioxide is one of the most attractive inorganic transition metal oxide materials from environmental and economic stand points. It is widely used in biosensors [10], catalysis [11], electrochromic multilayered nanocomposite thin films [12-13] and high-performance electrochemical electrodes and energy storage [14]. Typically, MnO is a transparent semiconductor that is conducting with an n-type carrier [15]. The pulsed laser deposition method involves ablating one or more targets that have been irradiated by a focused pulsed laser beam in order to produce thin films. This approach was originally used in 1965 by Smith and Turner [16]. Due to its outstanding chemical stability, transparency, low toxicity, low cost, functional biocompatibility, excellent adsorption capacity, catalytic capabilities, and global availability, nanostructured manganese dioxide (MnO) is a potential transition metal oxide [17]. The current study investigated the synthesis and characterization of optically transparent (MnO) films doped with different concentrations of Cu nanoparticles. The (MnO-Cu) thin films' structural, morphological, and optical characteristics were examined using UV-visible spectroscopy, atomic force microscopy, and X-ray diffraction (XRD).

2. EXPERIMENTAL

2.1 Preparation of Samples

Various concentrations of Cu nanoparticles (0.03, 0.05, 0.07, and 0.09 were used) were mixed with 99.99% pure MnO. In a gate mortar, the powder was mixed for five minutes. After that, it was compacted into pellets with a diameter of 1 cm and a thickness of 0.2 cm using a hydraulic press for 10 minutes at a pressure of 5 tons. After an hour of 400 °C sintering, the pellets were cooled to ambient temperature.

† ***Cite as:*** D.T. Mohammed, G.H. Mohammed, East Eur. J. Phys. 3, 391 (2023), https://doi.org/10.26565/2312-4334-2023-3-42

2.2 Deposition of Thin Films

The generated pellets were used to create thin films of (MnO)1-xCux on glass substrates with dimensions of 2.5×7.5 cm that had been cleaned employing an ultrasonic process and distilled water for 15 minutes. The pulsed laser deposition method was applied to produce thin films with the Nd:YAG laser. It produced 500 mJ of energy for 300 laser pulses that were incident on the target surface at a 45° angle and repeated at a frequency of 6 Hz. The deposition was done at (1-10-1) mbar of chamber pressure. The distance between the target and the substrate was 1.5 cm. The layer thickness of 200±5nm was estimated using the interference technique.

2.3 Measurements

By employing Cu-Ka (= 0.154 nm) throughout a 2-scan range of 10-80°, the structural properties of $(MnO)_{1-x}$ Cu_x thin films were studied by an X-ray diffractometer (Philips PW1730). Atomic force spectroscopy (AFM) was used to investigate the surface morphological characteristics of the film. Using a UV-Vis-NIR spectrophotometer with a 190-1100 nm wavelength range (Metertech SP8001), the optical characteristics of thin films were investigated.

3. RESULTS AND DISCUSSIONS

3.1 The X-rays Diffraction Results

Figure 1 displays the XRD patterns of different Cu concentrations in doped and undoped MnO thin films. The outcomes demonstrated the polycrystalline nature of the films. This outcome is consistent with Zahan et al. [18].

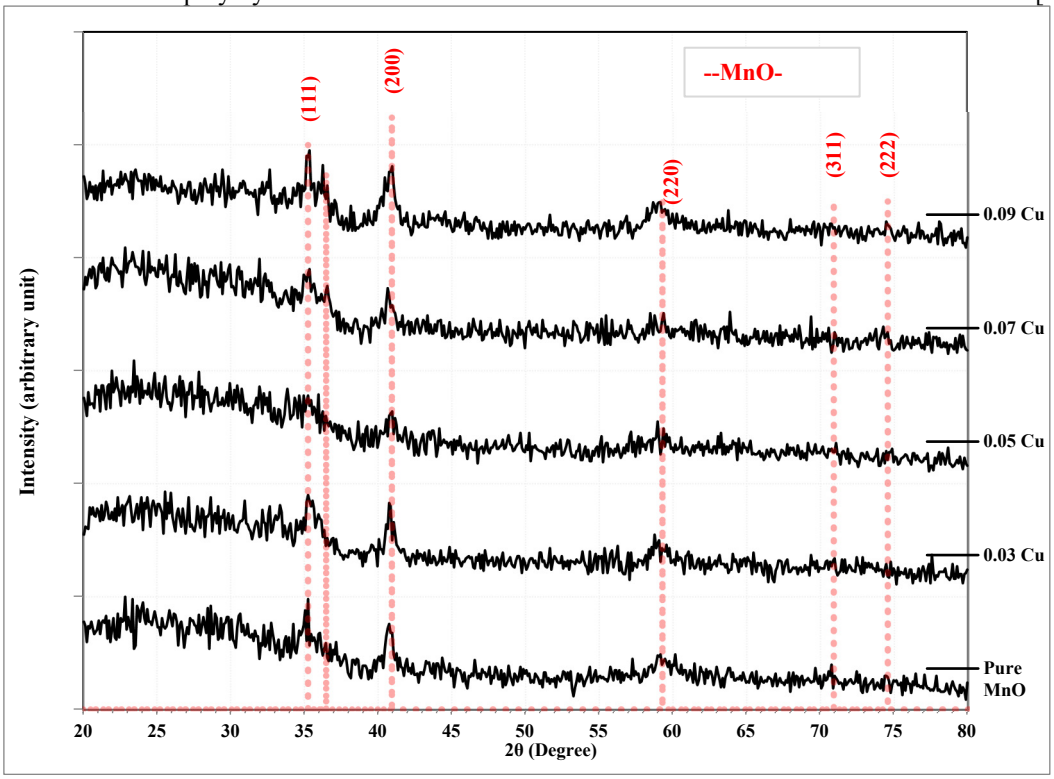

Figure 1. Shows the X-ray diffraction of Cu nanoparticles doped in different quantities in MnO

By comparing the results with ASTM card files (No. 96-900-6666), the diffraction peaks are identified. MnO-Cu thin films were discovered to have a cubic structure. There are two strong peaks and three other smaller ones in the X-ray diffraction spectra of MnO. It denotes the polycrystalline nature of the film. The strongest peak in the XRD pattern was at an angle of 35.31, which corresponds to a reflection of (111). It was observed that two additional strongest peaks developed at an angle of 40.85, which corresponded to a reflection of (200), when Cu with (0.05 and 0.07) content was added to the films. This demonstrates the impact of copper content. The Debye-Scherer equation was used to determine the crystal's size (Cs) [19-21].

$$C_S = \frac{0.9\lambda}{\beta \cos\theta}. \quad (1)$$

Where: θ the diffraction angle, $\boldsymbol{\beta}$ full width at half maximum (FWHM), and λ wavelength of the X-ray are all given.

In accordance with the Debye-Scherer equation as well. For (111) and (200), the findings are shown in Table 1. Average crystallite size, interplanar spacing, and the number of planes in the diffraction pattern of undoped and doped MnO thin films with various Cu contents Table 1 results showed that the average crystallite size had increased along with the increase in copper concentration. In contrast to earlier research, this study's findings revealed [18].

Table 1. Lists the crystal size, FWHM, and interplaner distance for (MnO) thin films doped with various concentrations of Cu nanoparticles.

Cu %	2θ (Deg.)	FWH M (Deg.)	dhkl Std.(Å)	C.S (nm)	hkl	Phase
MnO	35.10	0.7055	2.5548	11.8	(111)	Cubic MnO
MnO-Cu (0.03)	35.31	0.6349	2.5400	13.1	(111)	Cubic MnO
MnO-Cu (0.05)	40.85	0.7760	2.2072	10.9	(200)	Cubic MnO
MnO-Cu (0.07)	35.34	0.5643	2.5375	14.8	(111)	Cubic MnO
MnO-Cu (0.09)	35.31	0.2822	2.5400	29.6	(111)	Cubic MnO

3.2 Atomic force microscopic

Analysis of the surface morphology of films grown on glass substrates can be done by using 3D AFM images of MnO thin films doped with various concentrations of Cu nanoparticles to calculate the mean diameter, mean roughness, and mean square root (RMS). The fine morphology and roughness of the MnO films may be seen with various Cu activators. Roughness and RMS change increased with the addition of Cu, with a Cu ratio of 0.09 producing the maximum value. The 0.09 Cu ratio is the best among the other ratios, based on the findings of the XRD and AFM tests (it produced the highest roughness and largest crystalline size).

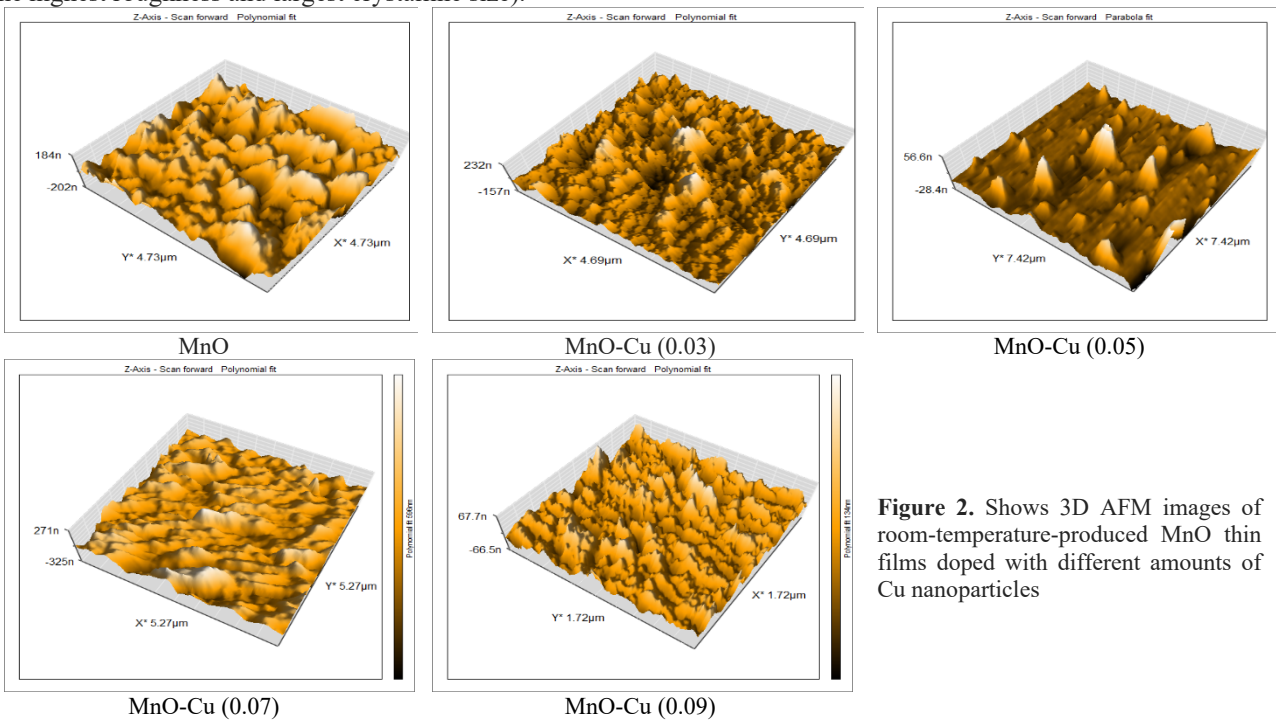

Figure 2. Shows 3D AFM images of room-temperature-produced MnO thin films doped with different amounts of Cu nanoparticles

Table 2. Granular content and total surface roughness of the produced films at room temperature

Sample	Avg.Diameter (nm)	Avg.Roughness (nm)	R.M.S (nm)	Peak-Peak (nm)
MnO	178.2	62.74	84.34	109.6
MnO-Cu (0.03)	44.17	37.40	45.41	96.13
MnO-Cu (0.05)	131.1	7.446	13.48	73.38
MnO-Cu (0.07)	58.97	59.76	76.15	228.4
MnO-Cu (0.09)	71.21	65.40	84.71	200.4

3.3 The optical properties

Undoped and doped (MnO) thin films with varying concentrations of Cu (0.03, 0.05, 0.07, and 0.09% wt.) were studied for transmission, absorption coefficient, extinction coefficient, refractive index, dielectric constant, and optical energy gap in the wavelength range of 500–1100 nm.For (MnO-Cu) produced at RT, Figure 3 depicts the transmission variation with wavelength. The image and Table 3 make it clear that the transmittance value is inversely proportional to the Cu concentration; as the Cu content in MnO films increased, so did the transmittance value.

The relation [22, 23] can be used to get the absorption coefficient:

$$\alpha = 2.303\,A/t\,. \tag{2}$$

where t is the sample's thickness and A is the absorbance. The following relation [24] can be used to compute the optical energy gap's value:

$$\alpha h\nu = B(h\nu - Eg)r, \tag{3}$$

where B is a constant inversely proportional to the degree of amorphousness, hv is the energy of the input photon, r is the exponent denoting the kind of optical transitions in the material, and Eg is the optical bandgap.

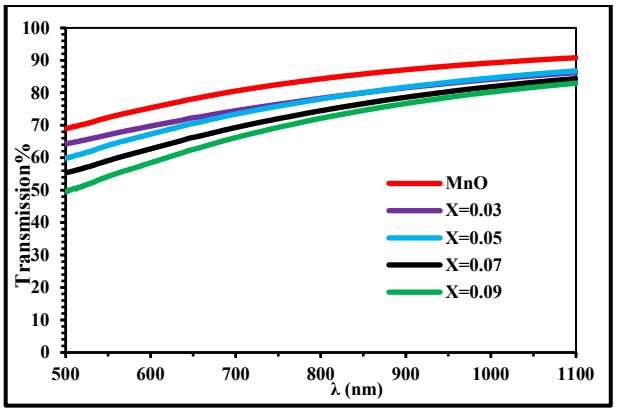

Figure 3. Shows the transmittance spectra of Cu nanoparticle-doped MnO thin films at various concentrations

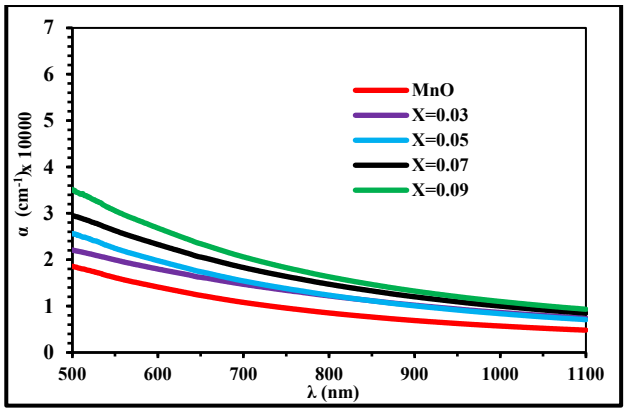

Figure 4. Shows the absorption coefficient of thin films of MnO doped with various concentrations of Cu nanoparticles

Band-to-band absorption causes a significant increase in an electron's absorption when it is moved up to the conduction band from the valence band, producing a new pair of charge carriers (an electron and a hole). The bandgap values for the various Cu contents are shown in Table 3. The absorbance increases as Cu concentration (x) increases and Eg decreases.

Table 3. Shows the transmittance, absorption coefficient, and optical constant of (MnO) thin films at room temperature that are both undoped and doped with (Cu) in the following ratios: 0.030.050.070.009.

Sample	T%	α (cm-1)	k	n	εr	εi	Eg (eV)
MnO	68.99	18561	0.074	2.257	5.088	0.333	2.69
MnO-Cu(0.03)	64.29	22085	0.088	2.370	5.609	0.417	2.6
MnO-Cu(0.05)	59.88	25640	0.102	2.463	6.057	0.503	2.4
MnO-Cu(0.07)	55.34	29585	0.118	2.543	6.454	0.599	2.23
MnO-Cu(0.09)	49.64	35018	0.139	2.614	6.815	0.729	2.19

Figure 5 shows that optical bandgap measurements fall from roughly 2.69 eV to 2.19 eV at room temperature when the Cu content increases from 0% to 9%.

Figure 6 shows the connection between the extinction coefficient (k) and wavelength in the 500-1100 nm range for samples made at room temperature, illustrating how the k values climb as the doping level increases. Table 3 provides an illustration of the results. The values of k were calculated based on the relationship shown in [25].

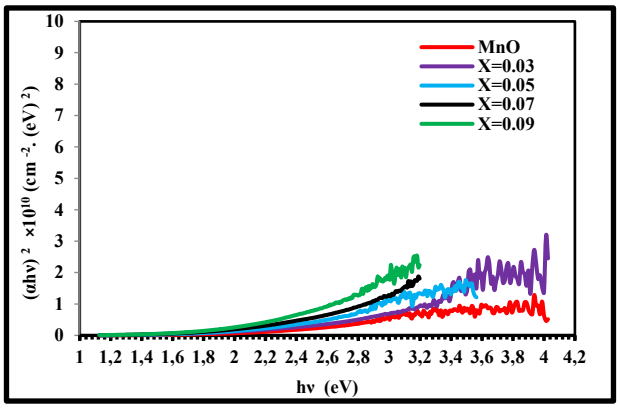

Figure 5. Shows the plot of $(\alpha h\upsilon)^2$ as a function of $(h\upsilon)$ for thin films of MnO doped with various concentrations of Cu nanoparticles

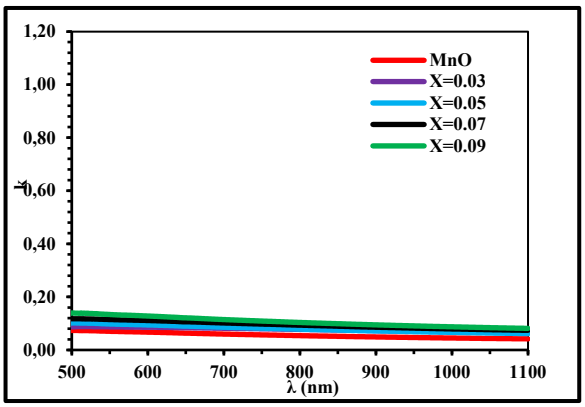

Figure 6. Shows the MnO thin films doped with various concentrations of Cu nanoparticles and their extinction coefficients (k)

extinction coefficients (k):

$$k = \frac{\alpha\lambda}{4\pi} \tag{4}$$

Figure 7 and Table 3 Show how the refractive index changes with wavelength for undoped and doped MnO with different amounts of Cu in the wavelength range of 500-1100 nm. It can be seen that the refractive index rises as the doping increases.

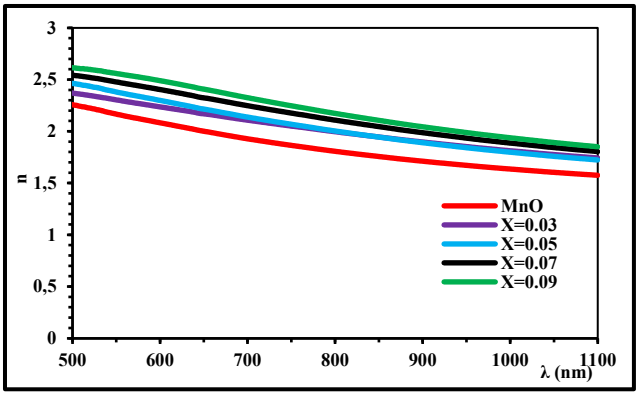

Figure 7. Shows the refractive index of thin films of MnO doped with various concentrations of Cu nanoparticles.

The complicated optical refractive index of thin films is described by equation (5) [26]:

$$n^* = n - ik \tag{5}$$

where (n) and (k) are the real portion and imaginary part of a complex refractive index, respectively, and (n*) is the complex refractive index. While the relationship [27] can be used to determine the simple refractive index:

$$n=\frac{1+R}{1-R}+\sqrt{\frac{4R}{(1-R)^2}-k^2}\ . \tag{6}$$

Figures 8 and 9 show the real and imaginary portions of the dielectric constant of undoped and doped (MnO) thin films with different Cu concentrations (0.03, 0.05, 0.07, and 0.09), respectively, in the wavelength range (500–1100 nm) at room temperature. Since (k2) is much smaller than (n2), part (per Equation 7) simply depends on the value of (n2).

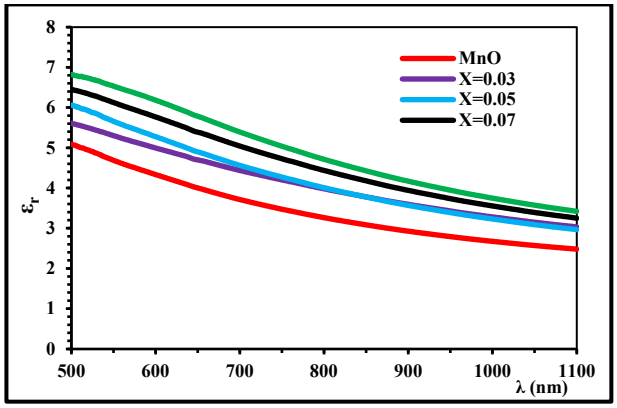

Figure 8. Shows the real component of the dielectric constant for thin films of MnO doped with various concentrations of Cu nanoparticles

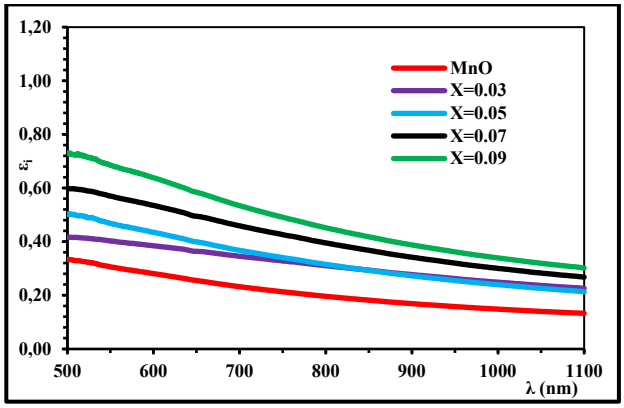

Figure 9. Shows the imaginary portion of the dielectric constant for thin films of MnO doped with various concentrations of Cu nanoparticles

The imaginary portion, however, is dependent on the value of (k) (see Equation 8). It was discovered that their values increased as the doping and wavelength were raised, as indicated in Table 3. Applying the equations [28], the real and imaginary components of the dielectric constant were computed.

$$\varepsilon_r = n^2 - k^2 \tag{7}$$

$$\varepsilon_i = 2nk \tag{8}$$

3.4 Hall Effect

Undoped and doped (MnO) thin films with varying Cu contents (0.03, 0.05, 0.07, and 0.09) wt were studied using Hall Effect measurements. Table (4) shows that all samples exhibit a positive negative Hall coefficient (i.e., n-type conductivity), with the exception of films doped at x = 0.05, 0.07, where the Hall coefficient sign has been transformed to p-type due to the high concentration of carriers. Additionally, the results demonstrate that a drop in the values of charge carriers (n) with a decrease in both the mobility (μ_H) and Hall coefficient (R_H) values causes an increase in the value of electrical conductivity (σ).

Table 4. Hall coefficient, Hall mobility, carrier concentration, and conductivity type for MnO films doped with various Cu at RT

Sample	σ (1/ Ω Cm)	ρ (Ω cm)	R_H(cm³/c)	n_H(1/cm³)	μ_H(cm²/v·sec)	type
MnO	3.12E+00	3.205E-01	-4.21E+01	-1.48E+17	1.32E+02	N
MnO-Cu(0.03)	1.22E+01	8.197E-02	-5.85E+01	-1.07E+17	7.14E+02	N
MnO-Cu(0.05)	2.83E+01	3.533E-02	2.90E+02	2.15E+16	8.21E+03	P
MnO-Cu(0.07)	2.47E+01	4.048E-02	4.20E+01	1.49E+17	1.04E+03	P
MnO-Cu(0.09)	3.44E+00	2.907E-01	-8.12E+01	-7.69E+16	2.79E+02	N

3.5 Current-Voltage Characteristics Measurements at Illumination

Show the J-V characteristics of the $(MnO)_{1-x}Cu_x$/Si heterojunction made by pulsed laser deposition at different Cu concentrations (x = 0.03, 0.05, 0.07, and 0.09) under ambient lighting (100 mW/cm2) at room temperature. The values of J-V parameters (Voc , Isc , Vm , Im , F.F and η) were tabulated in Table 5 . In general, it can be observed that the Isc decreases as the cu content increases. It is noticed a decrease in the values of the fill factor and the efficiency value as the Cu content increases and further result in a poor electrocatalytic performance this outcome is consistent with Peng et al. [29].

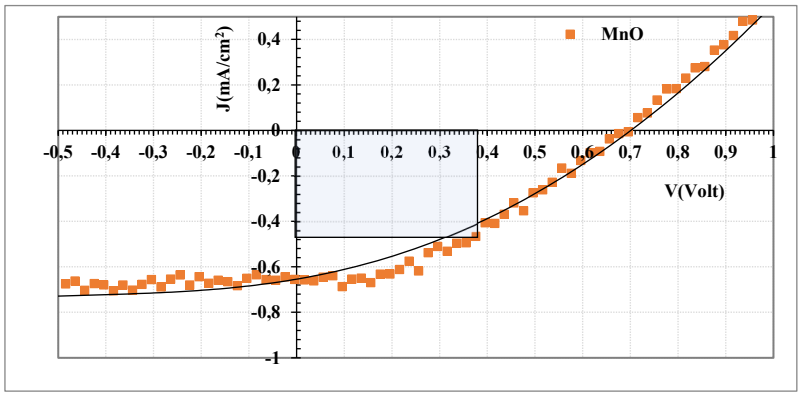

Figure 10. J-V characteristics under illumination by 100mW/cm² white light for MnO/p-Si at R.T.

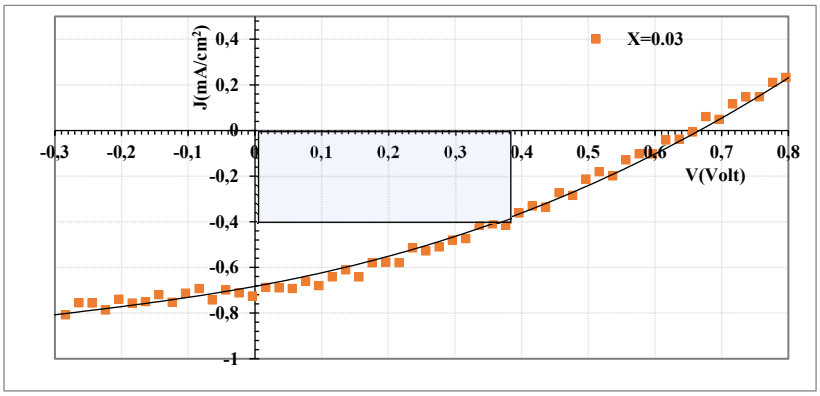

Figure 11. J-V characteristics under illumination by 100mW/cm² white light for $(MnO)_{1-x}$ Cu_x/p-Si with Cu content 3% at R.T.

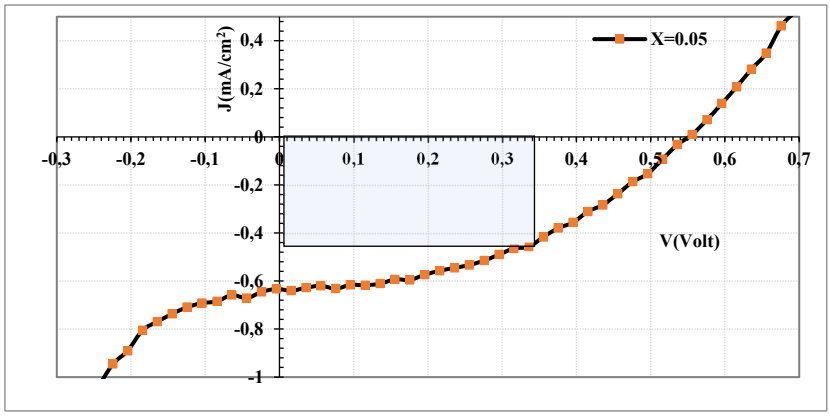

Figure 12. I-V characteristics under illumination by 100mW/cm² white light for $(MnO)_{1-x}$ Cu_x/n-Si with Cu content 5% at R.T.

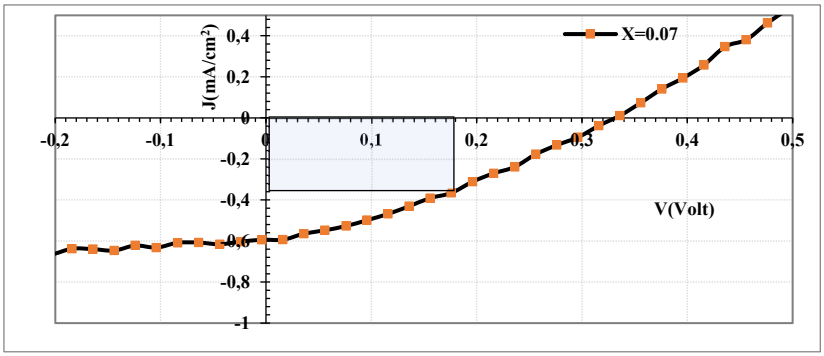

Figure 13. I-V characteristics under illumination by 100mW/cm2 white light for $(MnO)_{1-x}Cu_x$/n-Si with Cu content 7% at R.T.

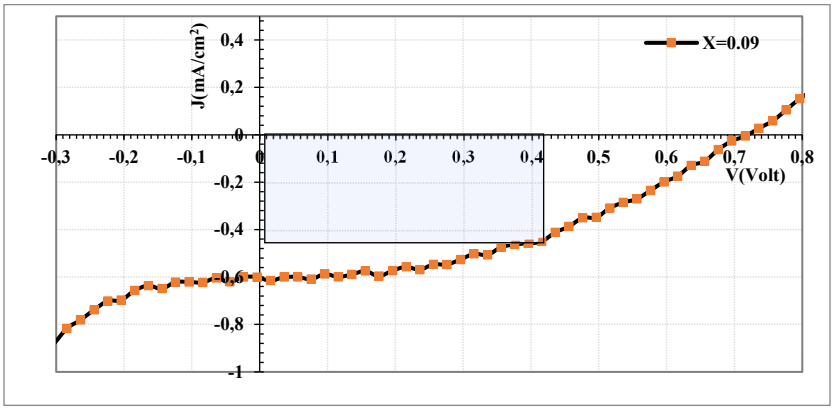

Figure 14. I-V characteristics under illumination by 100mW/cm^2 white light for $(MnO)_{1-x}Cu_x$/p-Si with Cu content 9% at R.T.

Table 5. Photovoltaic characterization (Voc, Isc, Vm, and Im) of $(MnO)_{1-x}$Cux/p and n-Si heterojunctions illuminated by 100mW/cm^2 white light with different Cu content prepared at RT

Sample	Isc (mA)	Im	Voc	Vm	FF	Pm (mW)	Efficincy (ɳ)
MnO	0.66	0.47	0.70	0.38	0.39	0.1786	0.18
MnO-Cu(0.03)	0.70	0.38	0.65	0.54	0.45	0.2052	0.21
MnO-Cu(0.05)	0.64	0.46	0.55	0.34	0.44	0.1564	0.16
MnO-Cu(0.07)	0.60	0.36	0.33	0.18	0.33	0.0648	0.06
MnO-Cu(0.09)	0.62	0.45	0.72	0.42	0.42	0.189	0.19

4. CONCLUSION

The impact of doping (MnO) thin films with various Cu contents on their structural, morphological, and optical features was investigated in the current work. The films' polycrystalline nature was demonstrated by the XRD pattern, which had the highest peak present at an angle of 35.31, which corresponded to a reflection of (111). The ratio of 0.09 percent Cu is the best among the other ratios, according to the XRD and AFM analyses (it produced the highest crystalline size and the highest roughness). The absorbance coefficient rose for all samples as the doping ratio rose. It was discovered that as the doping ratio grew, the refractive index, extinction coefficient, and dielectric constant (real and imaginary parts) all increased. Hall Effect measurement showed that films have n-type to all samples except (0.03 and 0.05) in RT. J-V characteristic showed the maximum efficiency which was 0.21% at MnO-Cu (0.03) at RT and the value of the filling factor decreases with doped Cu at (RT).

ORCID

Doaa T. Mohammed, https://orcid.org/0009-0001-7444-606X; **Ghuson H. Mohammed,** https://orcid.org/0000-0002-7401-3539

REFERENCES

[1] P.U. Asogwa, S.C. Ezugwu, F.I. Ezema, "Variation of optical and solid state properties with post deposition annealing in PVA-Capped MnO_2 thin films," Superficies y Vacio, **23**(1) 18-22 (2010). https://www.fis.cinvestav.mx/~smcsyv/supyvac/23_1/SV2311810.pdf

[2] D.K. Naser, A.K. Abbas, and K.A. Aadim, "Zeta potential of Ag, Cu, ZnO, CdO and Sn nanoparticles prepared by pulse laser ablation in liquid environment," Iraqi Journal of Science, 2570-2581 (2020). https://doi.org/10.24996/ijs.2020.61.10.13

[3] J. Medina-Valtierra, J. Ramrez-Ortiz, V.M. Arroyo-Rojas, and F. Ruiz, "Cyclohexane oxidation over Cu_2O–CuO and CuO thin films deposited by CVD process on fiberglass," Applied Catalysis A, **238**, 1-9 (2003). https://doi.org/10.1016/S0926-860X(02)00074-1

[4] R. Naeem, R. Yahya, A. Pandikumar, N.M. Huang, M. Misran, Z. Arifin, and M. Mazhar, "Photoelectrochemical properties of morphology-controlled manganese, iron, nickel and copper oxides nanoball thin films deposited by electric field directed aerosol assisted chemical vapor deposition," Materials Today Communications, **4**, 141-148 (2015). https://doi.org/10.1016/j.mtcomm.2015.06.004

[5] Z.S. Mahdi, and G.H. Mohammed, "Structural and Optical Properties of GO-doped (TiO_2: MoS_2) Films Prepared by Pulsed Laser Deposition," Journal of Survey in Fisheries Sciences, **10**(3S), 5658-5668 (2023). https://sifisheriessciences.com/journal/index.php/journal/article/view/1954/2010

[6] F.K. Allah, S.Y. Abe, C.M. Nunez, A. Khelil, L. Cattin, M. Morsli, J.C. Bernede, *et al*., "Characterisation of porous doped ZnO thin films deposited by spray pyrolysis technique," Applied Surface Science, **253**, 9241-9247 (2007). https://doi.org/10.1016/j.apsusc.2007.05.055

[7] O. Nilsen, H. Fjellvag, A. Kjekshus, "Growth of manganese oxide thin films by atomic layer deposition," Thin Solid Films, **444**, 44-51 (2003). https://doi.org/10.1016/S0040-6090(03)01101-5

[8] H. Unuma, T. Kanehama, K. Yamamoto, K. Watanabe, T. Ogata, M. Sugawara, "Preparation of thin films of MnO_2 and CeO_2 by a modified chemical bath (oxidative-soak-coating) method," Journal of Materials Science, **38**, 255-259 (2003). https://doi.org/10.1023/A:1021197029004

[9] M.A. Abood, and B.A. Hasan, "A Comparison Study the Effect of Doping by Ga_2O_3 and CeO_2 On the Structural and Optical Properties of SnO_2 Thin Films," Iraqi Journal of Science, **64**(4), 1675-1690 (2023). https://doi.org/10.24996/ijs.2023.64.4.10

[10] S. Liang, F. Teng, G. Bulgan, R. Zong, and Y. Zhu, "Effect of Phase Structure of MnO_2 Nanorod Catalyst on the Activity for CO Oxidation," Journal of Physical Chemistry C, **112**, 5307-5315 (2008). https://doi.org/10.1021/jp0774995

[11] M. Nakayama, Y. Kashiwa, and K. Suzuki, "Electrochromic Properties of MnO_2-Based Layered Polymer Nanocomposite," Journal of the Electrochemical Society, **156**, D125-D130 (2009). http://dx.doi.org/10.1149/1.3072896

[12] N. Sakai, Y. Ebina, K. Takada, and T. Sasaki, "Electrochromic Films Composed of MnO2 Nanosheets with Controlled Optical Density and High Coloration Efficiency," Journal of the Electrochemical Society, **152**, E384-E389 (2005). https://doi.org/10.1149/1.2104227

[13] D. Yuping, M. He, L. Xiaogang, L. Shunhua, and J. Zhijiang, "The microwave electromagnetic characteristics of manganese dioxide with different crystallographic structures," Physica B, **405**, 1826-1831 (2010). https://doi.org/10.1016/j.physb.2010.01.055

[14] A.K.M. Farid ul Islam, R. Islam, and K.A. Khan, "Studies on the thermoelectric effect in semiconducting MnO_2 thin films," Journal of materials science: Materials in electronics, **16**, 203-207 (2005). https://doi.org/10.1007/s10854-005-0766-1

[15] H. Xia, W. Xiao, M.O. Lai, and I. Lu, "Facile Synthesis of Novel Nanostructured MnO_2Thin Films and Their Application in Supercapacitors," Nanoscale Res. Lett. **4**, 1035–1040 (2009). https://doi.org/10.1007/s11671-009-9352-4

[16] R.K. Jamal, M.A. Hameed, and K.A. Adem, "Optical properties of nanostructured ZnO prepared by a pulsed laser deposition technique," Materials Letters, **132**, 31-33 (2014). https://doi.org/10.1016/j.matlet.2014.06.047

[17] K. Tian, M. Prestgard, and A. Tiwari, "A review of recent advances in nonenzymatic glucose sensors," Mater. Sci. Eng. C, **41**, 100-118 (2014). https://doi.org/10.1016/j.msec.2014.04.013

[18] Z. Muslima, and J. Podder, "Structural, optical and electrical properties of Cu: MnO_2 nanostructured thin films for glucose sensitivity measurements," SN Applied Sciences, **2**, 385-396 (2020). https://doi.org/10.1007/s42452-020-2191-8

[19] K.A. Aadim, R.A. Alansary, and S.A. Alhady, "Effect of Mn concentration on the structural and optical properties of SnO_2 thin films prepared by pulse laser deposition," Journal of Research and Method in Education (IOSR-JRME), **4**(4), 12-19 (2014). https://www.doi.org/10.9790/7388-04441219

[20] G.A. Al-Dahash, Q.M. Salman, and S.F. Haddawi, "Study the Effect of Copper (Cu) Doping on the Structure Properties of Zinc Oxide (ZnO) Prepared by Using Pulsed Laser Deposition (PLD)," J. Univ. Kerbala, **15**(2), 87-95 (2017). https://iasj.net/iasj/pdf/f612004da9aae7d2

[21] G.K. Williamson, and R.E. Smallman, "III. Dislocation Densities in Some Annealed and Coldworked Metals from Measurements on the X-Ray Debye-Scherrer Spectrum," Philos. Mag.: A journal of experimental and applied physics, **1**(1), 34-46 (1956). https://doi.org/10.1080/14786435608238074

[22] H. Kim, and C.M. Gilmore, "Transparent conducting aluminum-doped zinc oxide thin films for organic light-emitting devices," Appl. Phys. Lett. **76**(3), 259-261 (2000). https://doi.org/10.1063/1.125740

[23] S. Sami, S.S. Chiad, K. Haneen, T. Mubarak, N.F. Habubi, M.K. Mohammed, and A. Khadyair, "Fabrication and study the structure, optical and dispersion parameters of PMMA with $InCl_3$ additive," J. Glob. Pharma Technol. **11**(4), 369-374 (2019).

[24] M.G. Hutchins, O. Abu-Alkhair, M.M. El-Nahass, and K. Abd El-Hady, "Structural and optical characterisation of thermally evaporated tungsten trioxide (WO_3) thin films," Mater. Chem. Phys. **98**(2-3), 401-405 (2006). https://doi.org/10.1016/j.matchemphys.2005.09.052

[25] M. Thakurdesai, N. Kulkarni, B. Chalke, and A. Mahadkar, "Synthesis of CdSe Films by Annealing of Cd/Se Bilayer," Chalcogenide Lett. **8**(3), 223-229 (2011). http://chalcogen.ro/223_Thakurdesai.pdf

[26] S. Sönmezoğlu, A. Arslan, T. Serin, and N. Serin, "The effects of film thickness on the optical properties of TiO_2–SnO_2 compound thin films," Phys. Scr. **84**(6), 65602, 2011. https://doi.org/10.1088/0031-8949/84/06/065602

[27] A. Gultekin, "Effect of Au Nanoparticles Doping on The Properties of TiO_2 Thin Films," Materials Science (Medžiagotyra), **20**(1), 1392-1320 (2014). https://doi.org/10.5755/j01.ms.20.1.3709

[28] D. Na, L. Satyanarayana, G.-P. Choi, Y.-J. Shin, and J.S. Park, "Surface morphology and sensing property of NiO-WO_3 thin films prepared by thermal evaporation," Sensors, **5**(12), 519-528 (2005). https://doi.org/10.3390/s5120519

[29] A. Peng, Y. Gao, Q. Yang, X. Zuo, H. Tang, and G. Li, "MoC/MnO composite materials as high efficient and stable counter electrode catalysts for dye-sensitized solar cells," Journal of Materials Science: Materials in Electronics, **31**, 1976-1985 (2020). https://doi.org/10.1007/s10854-019-02717-8

ДОСЛІДЖЕННЯ СТРУКТУРНИХ, ОПТИЧНИХ ТА ЕЛЕКТРИЧНИХ ВЛАСТИВОСТЕЙ ЛЕГОВАНОГО MnO З МІДНИМИ ТОНКІМИ ПЛІВКАМИ, ПІДГОТОВЛЕНИМИ ЗА ТЕХНІКОЮ PLD ДЛЯ ЗАСТОСУВАННЯ У СОНЯЧНИХ ЕЛЕМЕНТАХ

Доаа Т. Мохаммед, Гусон Х. Мохаммед

Факультет фізики, Науковий коледж, Багдадський університет, Багдад, Ірак

У поточному дослідженні концентровані лазерні імпульси Nd:YAG при 500 мДж з другим випромінюванням при 1064 нм (ширина імпульсу 9 нс) і частотою повторення (6 Гц) для 300 лазерних імпульсів, що падають на поверхню мішені, використовувалися для покриття скляних підкладок тонкими плівками MnO. За допомогою рентгенівського дифрактометра (XRD), атомно-силового мікроскопа (АСМ) та спектрофотометра UV-Vis визначено структурні, морфологічні та оптичні характеристики плівок, легованих різними концентраціями Cu (0,03; 0,05; 0,07; і 0,09). Результати показують, що плівки є полікристалічними, з найбільшим піком, що з'являється під кутом 35,31, або дзеркальним (111). Кристалічний розмір осаджених тонких плівок був розрахований за допомогою формули Дебая-Шерера, і було виявлено, що він збільшується від 11,8 нм для нелегованого MnO_2 до 29,6 нм для легованого (MnO) зі збільшенням вмісту Cu від x=0 до x=0,09 за переважної орієнтації (111). Усі зразки мають кубічну структуру. Крім того, результати показали, що вміст Cu в плівках впливає на морфологію поверхні. За результатами АСМ-аналізу було виявлено, що шорсткість і середній діаметр змінюються при додаванні Cu до структури, причому найбільше значення спостерігається при співвідношенні Cu 0,09, що дорівнює 65,40 і 71,21 нм відповідно. Для дослідження оптичного пропускання використовували спектрофотометр UV–Vis. Було виявлено, що при збільшенні вмісту Cu в плівках пропускна здатність плівок зменшується. Вимірювання ефекту Холла показують, що всі підготовлені плівки при кімнатній температурі мають два типи провідності: p-тип і n-тип. Було вивчено електричні характеристики $(MnO)_{1-x}Cu_x$/PSi сонячної батареї з гетеропереходом і виявлено, що ефективність (η) зменшується зі збільшенням вмісту Cu.

Ключові слова: *наночастинки Cu; тонкі плівки MnO; техніка PLD; структурні властивості; оптичні властивості*